PTEN/AKT/mTOR pathway involvement in autophagy, mediated by miR-99a-3p and energy metabolism in ammonia-exposed chicken bursal lymphocytes

Syed Waqas Ali Shah,* Shuai Zhang,* Muhammad Ishfaq,† You Tang,‡ and Xiaohua Teng*,‡,1

*College of Animal Science and Technology, Northeast Agricultural University, Harbin 150030, People's Republic of China; †Heilongjiang Key Laboratory for Animal Disease Control and Pharmaceutical Development, Faculty of Basic Veterinary Science, College of Veterinary Medicine, Northeast Agricultural University, Harbin, People's Republic of China; and ‡Electrical and Information Engineering College, Jilin Agricultural Science and Technology University, Jilin, 132101, People's Republic of China

ABSTRACT Emission of atmospheric ammonia (**NH_3**) is an environmental challenge because of its harmful effects on humans and animals including birds. Among all organisms, NH_3 is highly sensitive to birds. Autophagy plays a critical role in Bursa of fabricius (**BF**)-mediated immune responses against various hazardous substances. Therefore, we designed our work to demonstrate whether NH_3 can induce autophagy in broiler chicken BF. In this study, the downregulated levels of mammalian target of rapamycin and light chain-3 (**LC-I**), as well as the upregulated levels of phosphate and tensin homology (**PTEN**), protein kinase B (**AKT**), autophagy related-5, light chain-3 (**LC3-II**), Becline-1, and Dynein, were found. Our results of transmission electron microscopy displayed signs of autophagosomes/autophagic lysosomes, and immunofluorescence assay displayed that NH_3 exposure reduced the relative amount of $CD8^+$ B-lymphocyte in chicken BF. Exposure of NH_3 led to energy metabolism disturbance by decreasing mRNA levels of glucose metabolism factors aconitase-2, hexokinase-1, hexokinase-2, lactate de hydrogenase-A, lactate dehydrogenase-B, pyruvate kinase, phosphofructokinase and succinate dehydrogenase complex unit-B, and adenosine triphosphates (**ATPase**) activities (Na^+/K^+ ATPase, Ca^{2+} ATPase, Mg^{2+} ATPase, and Ca/Mg^{2+} ATPase). Moreover, phosphate and tensin homology was found as target gene of microRNA-99a-3p which confirmed that high concentration of NH_3 caused autophagy in chicken BF. In summary, these findings suggested that ammonia induced autophagy via miR-99a-3p, the reduction of ATPase activity, and the alteration of autophagy-related factors, and energy metabolism mediation in BF. Our findings provide information to assess the harmful effects of NH_3 on chicken and clues for human health pathophysiology.

Key words: NH_3, autophagy, ATPase, miR-99a-3p, PTEN/AKT/mTOR signaling pathway

2021 Poultry Science 100:553–564
https://doi.org/10.1016/j.psj.2020.11.015

INTRODUCTION

Ammonia (**NH_3**) is a colorless, water soluble, irritant, and alkaline gas produced from the reduction of nitrogenous substances or bacterial decomposition of organic matters (Kristensen and Wathes, 2000). NH_3 originates mainly from agricultural sources, such as manures, slurries, and fertilizer applications (Behera et al., 2013). It is also emitted from nonagricultural sources including landfill sites, composting of organic materials, and combustion (Sutton et al., 2000). NH_3 is one of environmental pollutants, and its emission takes part in the formation of secondary inorganic aerosols which can lead to air pollution. It is well understood that air pollution caused by NH_3 emission has adverse effects on humans' and animals' health (Backes et al., 2016; Chen et al., 2020a). Based on adverse effects of NH_3 emission on health of workers and birds (Naseem and King, 2018), exposure limit of NH_3 in poultry houses was set as 25 ppm (Kristensen and Wathes, 2000). Some studies displayed the deleterious effects of high concentration of NH_3 on chicken small intestine mucosa, breast muscles, spleen, thymus, and liver (Zhang et al.,

Received May 3, 2020.
Accepted November 9, 2020.

[1]Corresponding author: tengxiaohua@neau.edu.cn

2015; Yi et al., 2016; An et al., 2019; Chen et al., 2019; Wang et al., 2019; Chen et al., 2020a; Xu et al., 2020). High concentration of NH_3 can cause disruption of glucose metabolism (Wang et al., 2019), liver damage, and autophagy in hepatocyte (Yan et al., 2018)

Autophagy is a catabolic process which can regulate innate and adaptive immunity (Deretic et al., 2013). Bursa of fabricius (**BF**) is a primary lymphoid organ (B-lymphopoiesis) of the birds responsible for humoral immunity (Jayachandra et al., 2017). A low level of autophagy in cells is normally in balanced condition, but this level may be enhanced when cells are stimulated by any foreign particle/stress, nutrient deficiency, or any other stimuli (Kroemer et al., 2010). For example, NH_3 is a known environmental stressor and can increase autophagy level in chickens' heart (Xing et al., 2019a). Previous studies demonstrated that cadmium, baicalin, and selenium led to autophagy, apoptosis, inflammation, and pyroptosis in rat liver, chicken lungs, ovarian, thymus, and carp pronephros tissues by altering the programmed death-related factors (Zou et al., 2015; Wang et al., 2018; Ishfaq et al., 2019; Hu et al., 2020; Sun et al., 2020; Zhang et al., 2020). Protein kinase B (AKT) and mammalian target of rapamycin (**mTOR**) were concerned with the regulation of autophagy process (Pant et al., 2017). Previous studies demonstrated the involvement of glucose metabolism factors (aconitase-2 [**ACO-2**], hexokinase-1 [**HK-1**], hexokinase-2 [**HK-2**], lactate dehydrogenase-A [**LDHA**], lactate dehydrogenase-B [**LDHB**], pyruvate kinase [**PK**], phosphofructokinase [**PFK**], and succinate dehydrogenase complex unit-B [**SDHB**]) in regulation of autophagy and apoptosis process (Lock et al., 2011; Moruno-Manchón et al., 2013; Wang et al., 2020), and it was also described that alteration in ATPase activity also concerns autophagy mediation (Rule et al., 2016; Yin et al., 2017). However, whether autophagy is involved in the toxicity caused by NH_3 is still elusive in chicken BF.

MicroRNAs (**miRNAs**), a type of small noncoding RNAs of approximately 22 nucleotides in length, can be involved in many biological processes including immunosuppression (Hu et al., 2019; Chen et al., 2020a,b,c,d). miR-30a and miR-30a-GRP78 Were involved in autophagy mediation (Singh et al., 2017; Shi et al., 2018). Xing and Han described the immune imbalance and autophagy induced by NH_3 inhalation–mediated miR-202-5p and miR-6615-5p in chicken heart and kidney (Xing et al., 2019a,b; Han et al., 2020a,b). A previous study described the involvement of miR-99a- and miR-99a-5p-mediated autophagy in mice heart and urinary bladder (Li et al., 2014; Tsai et al., 2018). Based on previous demonstrated works, we pretended that miR-99a-3p was involved in NH_3-induced autophagy in chicken BF. Thus, the present study was designed to investigate the mechanism of autophagy via determining miR-99a-3p; ATPase activities (Na^+/K^+ ATPase, Ca^{2+} ATPase, Mg^{2+} ATPase, and Ca/Mg^{2+} ATPase); mRNA levels of glucose metabolism factors (including ACO-2, HK-1, HK-2, LDHA, LDHB, PK, PFK, and SDHB); mRNA levels of autophagy-related genes (including phosphate and tensin homology [**PTEN**], mTOR, AKT, autophagy-related gene-5 [**ATG-5**], light chain-3 [**LC3**-I and LC3-II], Becline-1, and Dynein); and protein levels of energy metabolism and autophagy-related genes (ACO-2, HK-1, SDHB; Becline-1, PTEN, p-TOR/mTOR, p-AKT/AKT) to help in exploring the mechanism of NH_3 toxicity.

MATERIALS AND METHODS

Dose Management of NH3 Exposure to Animals

Institutional Animal Care and Use Committee of Northeast Agricultural University (Harbin, China) approved the present study. Ross 308 broiler chicks (135) were purchased from (Weiwei Co., Ltd., Harbin, China). The broiler chicks were randomly divided into 3 groups (45 birds in each group, 3 replication each group). Being given free access to drinking water and standard commercial diets, the broilers of 3 groups were kept in safe cages at the Experimental Animal Center in College of Veterinary Medicine, Northeast Agricultural University. The broiler chickens were exposed to NH_3 with the following concentrations (5 mg/m^2 for the low-NH_3 group, 10–15 mg/m^2 for the middle NH_3-treated group, and 20–45 mg/m^2 for the high NH_3-treated group). A cylinder of compressed anhydrous NH_3 (Dawn Gas Co., Ltd., Harbin, China) and a Photoacoustic Field Gas-monitor Innova-1412 (Lumasense Technologies, Inc., Santa Clara, CA) were used for the maintenance and control of NH_3 emission.

Transmission Electron Microscopic Observation

Transmission electron microscopic observation was performed according to our previous studies (Han et al., 2020a,b). The samples were fixed in 2.5% glutaraldehyde and washed in 0.2 mol phosphate buffer (pH = 7.2) for 15 min twice. Then, these samples were fixed in 1% osmium-tetroxide buffer for 60 min and were dehydrated in a gradual series alcohol (75–95%) and set in epoxy-glue. Finally, ultrathin pieces were stained with uranyl-acetate. The morphological changes of tissue samples were observed under transmission electron microscope (**TEM**) (Hitachi 7650; Hitachi, Tokyo, Japan).

Sample Collection for Determination of NH_3-Affected BF

Forty-five broiler chickens were randomly selected from each group and slaughtered at 14th, 28th, and 42nd d. BF samples were immediately separated and washed with ice cold phosphate buffer (PBS, pH = 7.2), frozen in liquid nitrogen, and stored at −80°C for further experimental work.

Immunofluorescence Microscopy for $CD8^+$ B-Lymphocyte Determination

IF assay was performed via incubating 5-micron-thick sections in xylene for 15 min. The sections were

Table 1. Specific primers used in RT-qPCR.

Genes	Forward primer (5′-3′)
ACO2	CCTGTGGACAAGCTGAGCATCG
	CTGCGACTCGTTGAAGGTGTGG
HK1	TCATGGCTGTTGTGAACGATACCG
	GGTCAATGTGCCGCATCTCCTC
HK2	TGGAGGTGAAGCGGAGGATGAG
	GCACCAGCAGCACACGGAAG
LDHA	TGCCTGTCTGGAGCGGAGTG
	GTCCACCACCTGCTTGTGAACC
LDHB	GCAGGTGTTCGTCAGCAAGAGG
	GGCAGGCCACTCAACTTCCATG
SDHB	TGGACGGACTCTATGAGTGCATCC
	TTGAAGTTGTGCCAGGCGTTCC
PK	CTCAGCCAACTCTCCGTGATATGC
	TCCACTGCTTCCAAGAACGATGAC
PFK	GTGAGAGTTGGCATAACGGAAGGC
	CGCATCTGGTCAGCAATCTTCTCC
AKT	ATGGAATGGACGAAGAGG
	ATCCGTGGACGATACTGG
mTOR	TGCGGAGTATGTGGAGTT
	GCTGGAAGAAGAATGTAGGT
AGT5	GGCACCGACCGATTTAGT
	GCTGATGGGTTTGCTTTT
LC3-I	TTACACCCATATCAGATTCTTG
	ATTCCAACCTGTCCCTCA
LC3-II	AGTGAAGTGTAGCAGGATGA
	AAGCCTTGTGAACGAGAT
PTEN	CTGCCAGACATGACCGCCATC
	AGGTCCAGGTCGAAGCCATCC
Dynein	CGGCTTGACCTATGGAATCT
	CATCACTGCGAGGAACTGC
Beclin1	TCTGAGCATAACGCATCTGG
	CGACTGGAGCAGGAAGAAG
β-actin	CCAGCCATGTATGTAGCCATCCAG
	ACGGCCAGCCAGATCCAGAC
gga-miR-99a-3p	GCGCAAGCTCGCTTCTATGGGTCT
U6	CACGCAAATTCGTGAAGCGTTCCA

Specific primers used in RT-qPCR.

dehydrated in ethanol (75 and 85%) for 5 min and washed in dH_2O; immersed in EDTA antigen retrieval buffer (pH 8.0); and maintained at boiling temperature for 7 to 8 min. To prevent the buffer solution from evaporation, the samples were cooled in PBS (pH 8.0) for 5 min using a rocker device. Liquid blocking pens were used to stop liquid elimination. After being incubated in spontaneous fluorescence quenching reagent for 5 min and being washed in fresh water, they were again incubated with primary antibody (diluted with PBS) goat-serum at room temperature and then with anti-CD8α antibodies (1:500 Biomos; Technology Co., Ltd., Beijing, China) in blocking solution at 4°C overnight, and then again incubated with FITC (1:400 Services-bio Co., Ltd., Wuhan, China) labeled antirabbit igG and mounted with DAPI (Beyotime Biotechnology, Co., Ltd., Jiangsu, China). Finally, the slides were observed under an inverted microscope (Nikon TE2000, Tokyo, Japan).

Measurement Na^+/K^+, Ca^{2+} and Ca/Mg^{2+} -ATPase

ATPase activities (including Na^+/K^+ ATPase, Ca^{2+} ATPase, Mg^{2+} ATPase, and Ca/Mg^{2+} ATPase) were determined according to manufacturer's instructions (Cat No. A016-2; Nanjing Jiancheng Bioengineering Institute, China). Molybdenum blue spectrophotometric technique was used to obtain the production of inorganic phosphorus from adenosine triphosphate (**ATP**) to adenosine diphosphate (**ADP**) at 660 nm. Hydrolysis of phosphate radicals was inhibited by adding other types of ATPase while performing one type of ATPase activity. To avoid interassay variations, the assay for each sample was conducted twice.

Detection of miRNA and mRNA Levels by qRT-PCR

The extraction of RNA (Li et al., 2019) from all experimental groups was performed with RNAiso Plus reagents (Takara, Japan). RNA quality was measured using a microultraviolet spectrophotometer (GeneQuant 1300/100; GE Healthcare Life Sciences, Sweden) at 260/280 ratio. Reverse transcription (**RT**) of miRNA was performed with miRcute Plus miRNA qPCR kit (Cat No. FP411; TIANJIN BIOTECH CO., LTD., Beijing, China) according to manufacturer's instructions. RT of mRNAs was performed with RT reaction system (60 μL) according to manufacturer's instructions (HaiGene, Harbin, China). The quantitative real-time PCR reaction condition was the same as our previous experiments (Shah et al., 2020a) and according to the manufacturer's instructions (HaiGene, Harbin, China). All primers were synthesized by Sangon Biotech Co., Ltd. (Shanghai, China) and are shown in (Table 1). The miRNA and mRNA levels were calculated according to Pfaffl's method (Pfaffl, 2001; Xing et al., 2019b). U6 and β-actin were used as internal control genes.

Western Blotting for Detection of Protein Levels

Protein extraction was performed using the Western blotting technique (Shah et al., 2020b). Proteins were loaded on sodium dodecyl sulfate-polyacrylamide gel (SDS-PAGE, 12%) to separate and shifted to nitrocellulose membranes. After being blocked with 5% non-fat milk in TBST for 2 h and being incubated with diluted primary chicken antibodies including LC3 (1:500), Beclin-1 (1:1,000), PTEN (1:1,000), AKT (1:500), β-actin (1:1,000), mTOR (1:500) (ImmonuWay), and ACO-2, HK-1 and SDHB (1:1,000) at 1 h for 37°C, then the membranes were washed 4 times with PBST for 5 min each time and were incubated in horseradish peroxidase–conjugated secondary antibodies against rabbit IgG (1:2000; Santa Cruz, CA) at 37°C for 1 h. Enhanced chemiluminescence (ELC Biosharp Life Sciences, Anhui, China) and image J software (National Institute of Health, Bethesda, MD) were used for the visuals of bound immune complexes.

Statistical Analysis

One-way ANOVA was used to determine the statistical significance ($P < 0.05$) among different experimental groups at the same time point and among different time points in the same group, followed by least significant

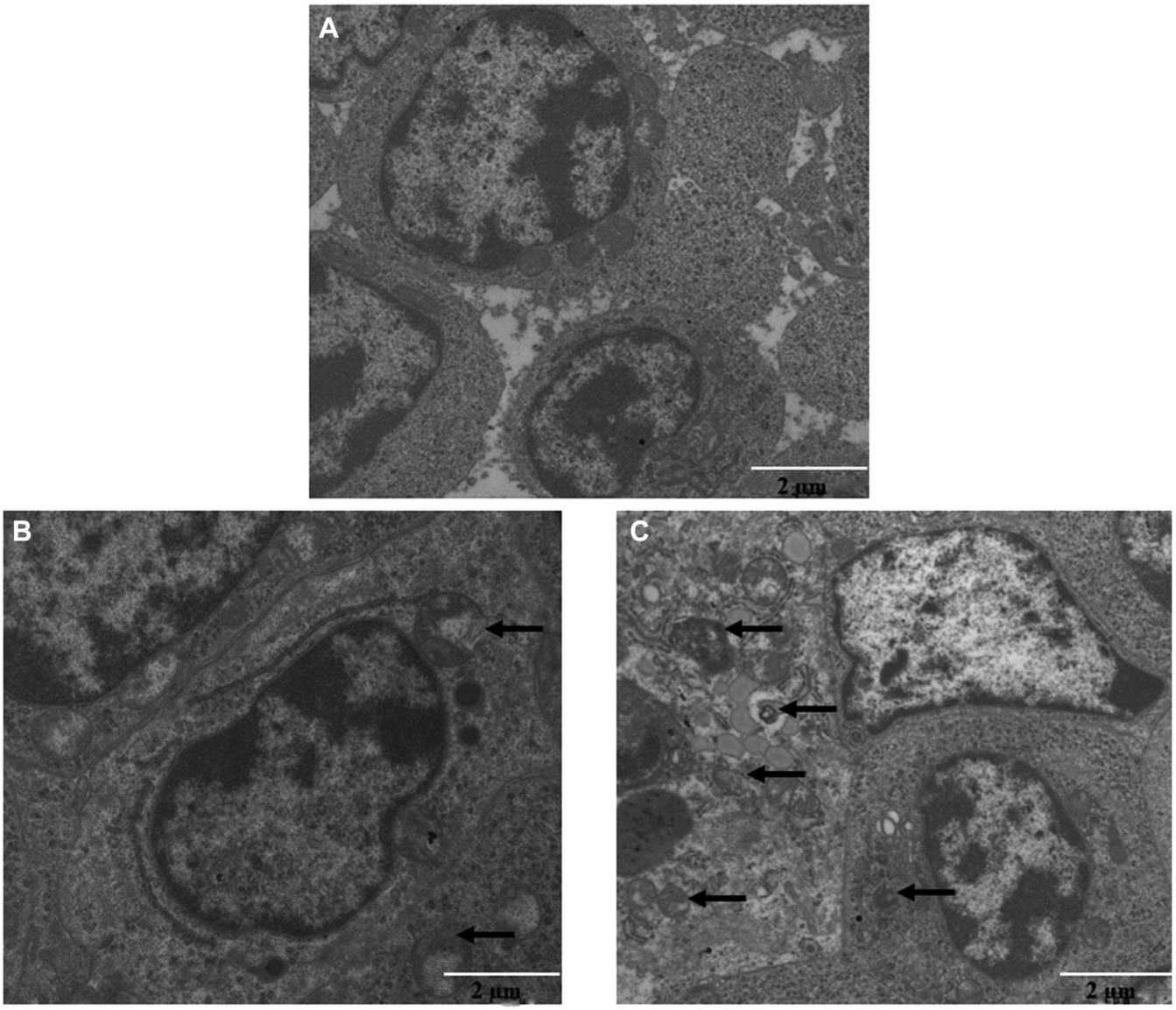

Figure 1. Detection of autophagosome formation by TEM. Experimental groups displayed as low, middle, and high NH_3-treated groups. The black arrows indicate autophagosomes/autophagic lysosomes in cytoplasm.

difference test through the statistical package for social science (SPSS window version 21.0, Chicago, IL). Heat map was made using heat map illustrator software (Heml, version, 1.0.3.7). GraphPad prism software (window version 6.01; San Diego, CA) was used to make all the graphs, and data were expressed as mean ± SD.

RESULTS

Ultrastructural Observation

TEM in autophagy research is the only tool that reveals the morphology of autophagic structures in nanometer resolution and represented their structures in natural environment and position among all other cellular components which allows their exact identification (Lucocq and Hacker, 2013). In this regard, the present study observed ultrastructures of chickens BF as shown in Figure 1. TEM observation showed formation of autophagosomes/lysosomes in the middle and high NH_3-treated groups (Figures 1B, 1C) is much more than that in the low NH_3 group (Figure 1A). The low NH_3 group displayed normal morphology (Figure 1A).

NH_3 Effects on Relative Levels $CD8^+$ B-Lymphocyte

We determined the relative levels of $CD8^+$ B-lymphocyte in chicken BF tissues by IF assay, as shown in Figure 2. The low NH_3 group showed normal amount of relative $CD8^+$ B-lymphocyte in chicken BF tissues (Figure 2A). However, a reduced amount of $CD8^+$ B-lymphocyte was found in the middle and high NH_3-treated groups (Figures 2B, 2C).

ATPase Activities

ATPase is a class of enzymes involved in the decomposition of ATP to ADP. So, we investigated ATPase

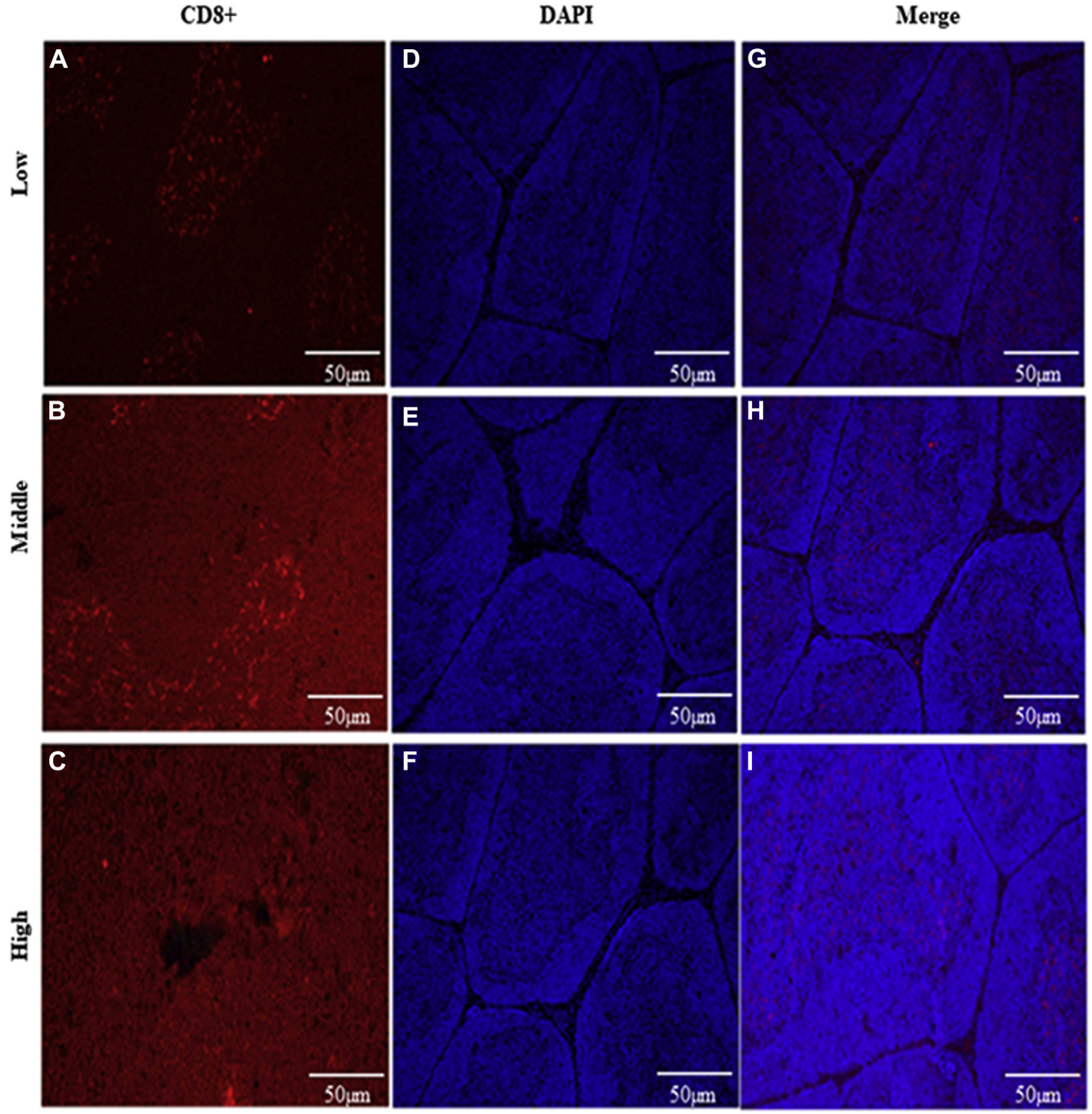

Figure 2. The estimation of $CD8^+$ B-lymphocyte by immunofluorescent assay in broilers BF. Experimental groups displayed as low, middle, and high (A–I) NH_3-treated groups.

activities (including Na^+/K^+ ATPase, Ca^{2+} ATPase, Mg^{2+} ATPase, and Ca/Mg^{2+} ATPase) in NH_3-treated chicken BF. The ATPase activities of chicken BF were shown in Figure 3. Our results displayed significant decrease ($P < 0.05$) in the activities of Na^+/K^+ ATPase (Figure 3A), Ca/Mg^{2+} ATPase (Figure 3B), Ca^{2+} ATPase (Figure 3C), and Mg^{2+} ATPase (Figure 3D) in the middle and high NH_3-treated groups compared with the low NH_3 group at all assessed time points. With the increase in NH_3 exposure time, ATPase activities of Na^+/K^+ ATPase and Ca^{2+} ATPase were significantly decreased ($P < 0.05$) at 28th and 42nd d, while Ca/Mg^{2+} ATPase and Mg^{2+} ATPase were significantly decreased ($P < 0.05$) at the 42nd d.

mRNA and Proteins Levels of Glucose Metabolism Factors

Relative mRNA and proteins levels of glucose metabolism factors in chicken BF are shown in Figure 4; mRNA levels, ACO-2 (Figure 4A), LDHA (Figure 4D), LDHB (Figure 4E), PFK (Figure 4F), PK (Figure 4G), and SDHB (Figure 4H) were significantly decreased

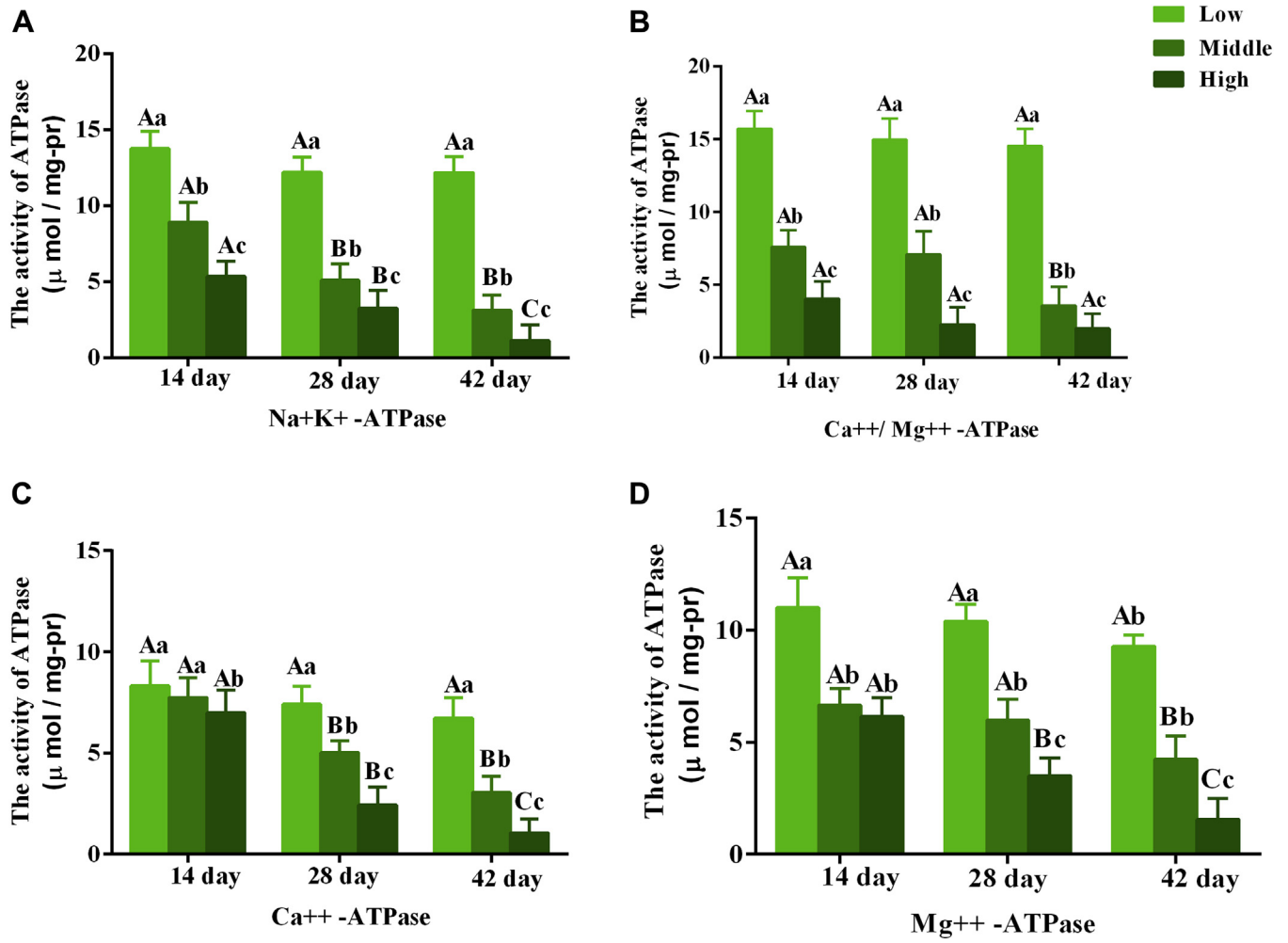

Figure 3. ATPase activities were measured at 14th, 28th, and 42nd d in all experimental groups. Experimental groups displayed as low, middle, and high NH_3-treated groups. (A) Na^+/K^+ ATPase, (B) Ca^{++}/Mg^{++} ATPase, (C) Ca^{++} ATPase, and (D) Mg^{++} ATPase. Bar graphs represent data with mean ± SD. Uppercase alphabets displayed significant difference ($P < 0.05$) of same group at different conducting time, and lowercase alphabets displayed significant difference ($P < 0.05$) of different groups at the same time.

($P < 0.05$) in the high NH_3-treated group compared with those in the low NH_3 group. Meanwhile, HK-1 and HK-2 were significantly decreased ($P < 0.05$) in the middle and high NH_3-treated groups compared with those in the low NH_3 group (Figures 4B, 4C) at all assessed time points. On the other hand, LDH, PFK, and SDBH were significantly ($P < 0.05$) decreased at 28th and 42nd d compared with those at the 14th d, while PK was significantly decreased ($P < 0.05$) at the 42nd d compared with that at 14th and 28th d. With respect to protein levels, ACO-2 displayed a significant decrease ($P < 0.05$) in the high NH_3-treated group compared with that in the low and middle NH_3-treated groups, while HK-1 and SDHB showed a significant decrease ($P < 0.05$) in the high and middle NH_3-treated groups compared with that in the low NH_3 group (Figure 4I).

Relative Levels of miR-99a-3p and Its Target Gene

The effect of NH_3 exposure on miR-99a-3p and its target gene PTEN are shown in Figure 5. miRNAs Performed their biological action in animal cells primarily by regulating the levels of target genes. We predicated a target gene for miR-99a-3p via a database potential targets. Our predicated data identified PTEN as the target gene for miR-99a-3p. The predicted site of target gene PTEN and miRNA are shown in Figure 5A. Our results of miR-99a-3p expression displayed a significant decrease ($P < 0.05$) in the middle and high NH_3-treated groups compared with that in the low NH_3 group (Figure 5B). However, mRNA level of PTEN was significantly increased ($P < 0.05$) in the middle and high NH_3-treated groups compared with that in the low NH_3 group (Figure 5C).

Relative Levels of Autophagy-Related Factors

Relative mRNA and protein levels of autophagic factors are shown in Figure 6. The mRNA levels of Dynein, ATG-5, and Beclin-1 were significantly increased ($P < 0.05$) in the high NH_3-treated group compared with those in the low and middle NH_3-treated groups

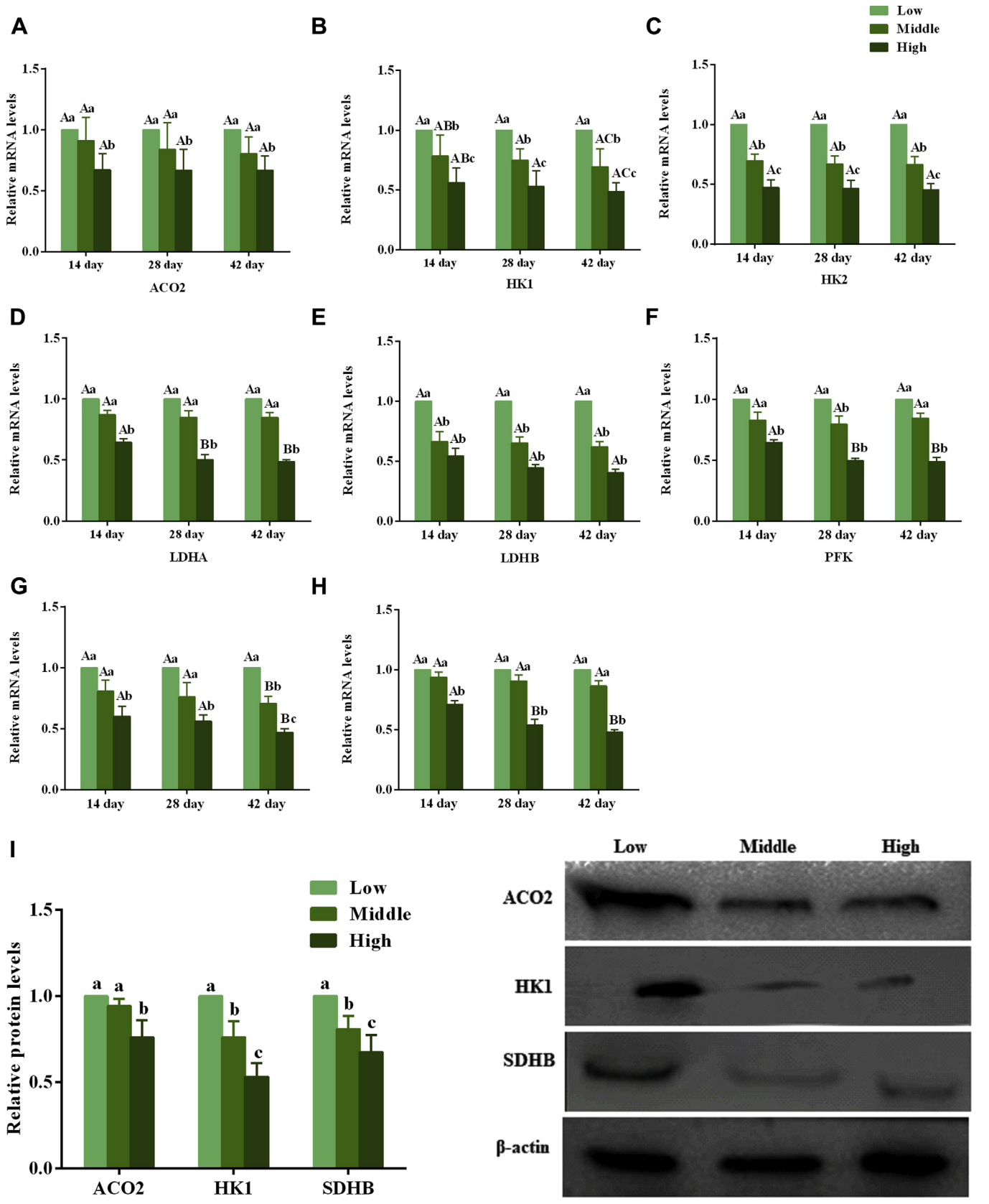

Figure 4. Relative mRNA ACO-2 (A), HK-1 (B), HK-2 (C), LDHA (D), LDHB (E), PFK (F), PK (G), and SDHB (H) and protein levels (I) of glucose metabolism factors in chicken BF. Experimental groups were displayed as low, middle, and high NH3-treated groups. Bar graphs represent data with mean ± SD. Uppercase alphabets displayed significant difference ($P < 0.05$) of same group at different conducting time, and lowercase alphabets displayed significant difference ($P < 0.05$) of different groups at same conducting time.

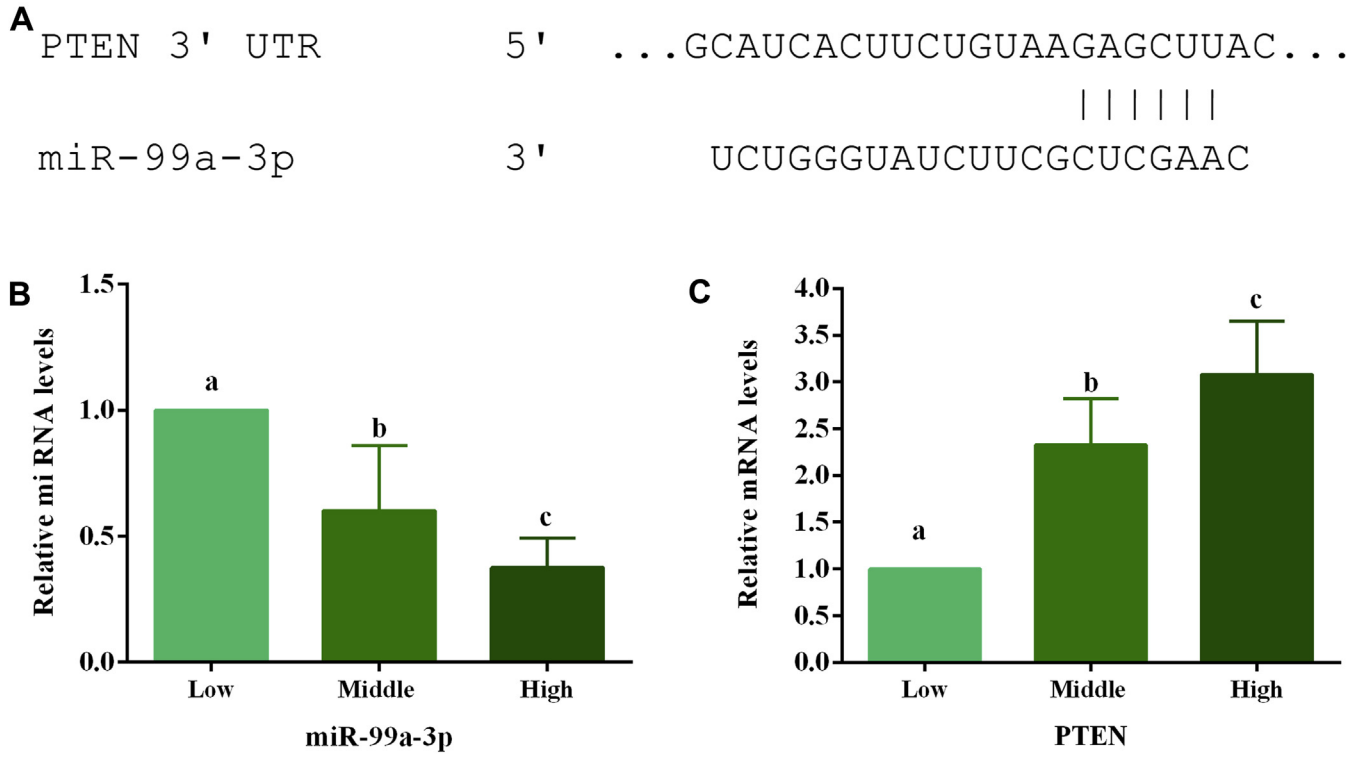

Figure 5. Relative miR-99a-3p and PTEN levels in chicken BF. Experimental groups displayed as low, middle, and high NH_3-treated groups. (A) alignment of miR-99a-3p with the predicted target region PTEN 3′ UTR, (B) levels of miR-99a-3p, and (C) levels of PTEN. Bar graphs represent data with mean ± SD. Uppercase alphabets displayed significant difference ($P < 0.05$) of same group at different conducting time, and lowercase alphabets displayed significant difference ($P < 0.05$) of different groups at same conducting time.

(Figures 6A, 6B, 6D). In addition, the levels of AKT and LC3-II were significantly increased ($P < 0.05$) in the high and middle NH_3-treated groups compared with the low NH_3 group (Figures 6C, 6E). Meanwhile, mRNA level of LC3-I was significant decreased ($P < 0.05$) in the middle- and high NH_3-treated groups compared with that in the low NH_3 group (Figure 6F). However, relative level of mTOR was significantly decreased ($P < 0.05$) in the high NH_3-treated group compared with that in the low and middle NH_3-treated groups (Figure 6G). During NH_3 exposure, the levels of Dynein, AGT-5, and AKT were significantly increased ($P < 0.05$) at the 42nd d compared with those at 14th and 28th d, while relative level of Beclin-1 was significantly increased at 28th and 42nd d compared with that at 14th d. Relative protein levels of Beclin-1 and PTEN were significantly increased ($P < 0.05$) in the middle- and high NH_3-treated groups compared with those in the low NH_3 group. Meanwhile, relative levels of p-AKT/AKT and p-mTOR/m-TOR were significantly decreased ($P < 0.05$) in the middle and high NH_3-treated groups compared with those in the low NH_3 group (Figure 6H).

Heat Map

A heat map of autophagy and glucose metabolism–related factors is shown in Figure 7. This heat map is a graphical representation of data where the individual values are contained in a matrix and represented as colors.

DISCUSSION

Autophagy is generally a good process for cell survival in adverse environments. NH_3, as a potential toxic byproduct in amino acid catabolism, plays an important role in inducing autophagy (Eng et al., 2010; Coltart et al., 2013; Tranah et al., 2013). Therefore, relevant cytological effects should be explored. After verifying that NH_3 can induce autophagy (Eng et al., 2010), we further analyzed the influence of NH_3 on $CD8^+$ B-lymphocyte, ATPase, energy metabolism, and miR-99a-3p and PTEN/AKT/mTOR expression and found that miR-99a-3p and PTEN/AKT/mTOR participated in stress reaction. Our results (Figures 5, 6) suggested that NH_3 facilitates the expression and activation of miR-99a-3p and autophagy-related genes (PTEN, mTOR, AKT, ATG-5, LC3-I/II, Becline-1, and Dynein), which are key factors of autophagy induction. Autophagy can be both selective and nonselective, and TEM can be used to monitor both (Yan et al., 2018). A previous study demonstrated the NH_3 induced autophagy in hepatocyte with formation of autophagosomes/autophagic lysosomes in their cytoplasm by TEM observation (Yan et al., 2018). Our results of TEM observation (Figure 1) were consistent with the aforementioned work and displayed signs of autophagosomes/lysosomes in all NH_3-treated groups. According to previous studies, the decreased level of $CD8^+$ lymphocytes resulted in the activation of autophagy (Xu et al., 2014). For example, *Mycoplasma gallisepticum* infection and NH_3 exposure reduced $CD4^+$ and $CD8^+$ lymphocytes

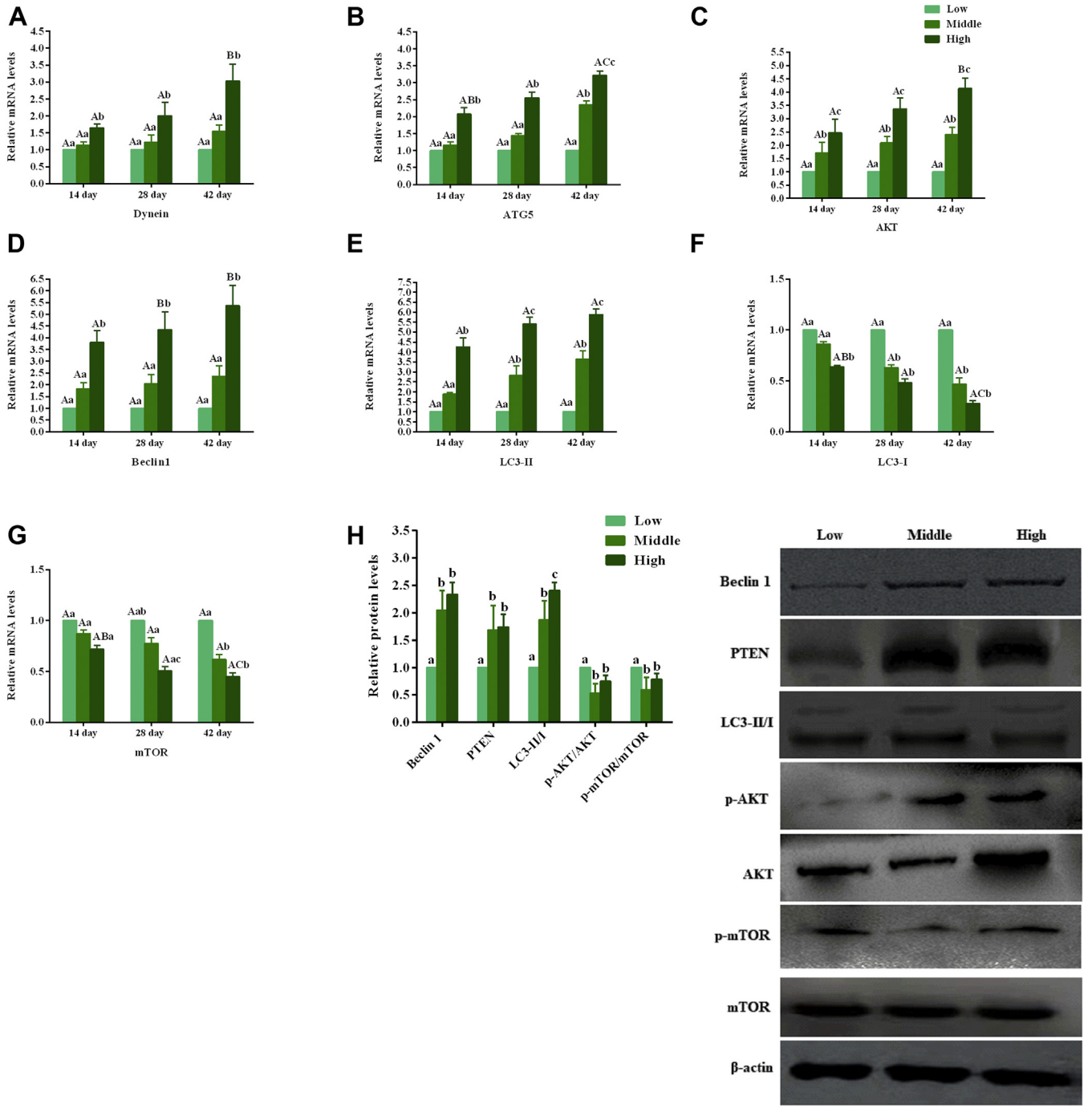

Figure 6. Relative mRNA and protein levels of autophagy-related genes in chicken BF. Experimental groups were displayed as low, middle, and high NH_3-treated groups. Bar graphs represent data with mean ± SD. Uppercase alphabets displayed significant difference ($P < 0.05$) of same group at different conducting time, and lowercase alphabets displayed significant difference ($P < 0.05$) of different groups at same conducting time.

numbers in dendritic cells of mice lungs and chicken BF and thymus (Luo et al., 2014; Tualeka and Jalaludin, 2018; Chen et al., 2020a; Zhang et al., 2020). Our results with IF assay (Figure 2) displayed reduced $CD8^+$ B-lymphocyte numbers in the middle and high NH_3-treated groups compared with that in the low group which showed that a decrease in $CD8^+$ B-lymphocyte leads to autophagy caused by NH_3 in chicken BF.

ATPase is important for energy production in cellular functions (Rule et al., 2016). Previous studies demonstrated that decrease in ATPase levels can lead to autophagy (Yin et al., 2017). Ammonia (NH_3) is one of the causative agents for decrease in ATP level by disrupting energy metabolism (Wang et al., 2019). Similar to NH_3, cadmium also reduced ATPase activities of chicken ovarian tissues (Wang et al., 2018). Similarly, decreased levels of ATPase (Na^+/K^+ ATPase, Ca^{2+} ATPase, Mg^{2+} ATPase, and Ca/Mg^{2+} ATPase) activities (Figure 3) were noted in BF tissues of chicken treated with NH_3.

Energy metabolism-related factors HK-II and PK have an important role in glycolysis (glucose breakdown)

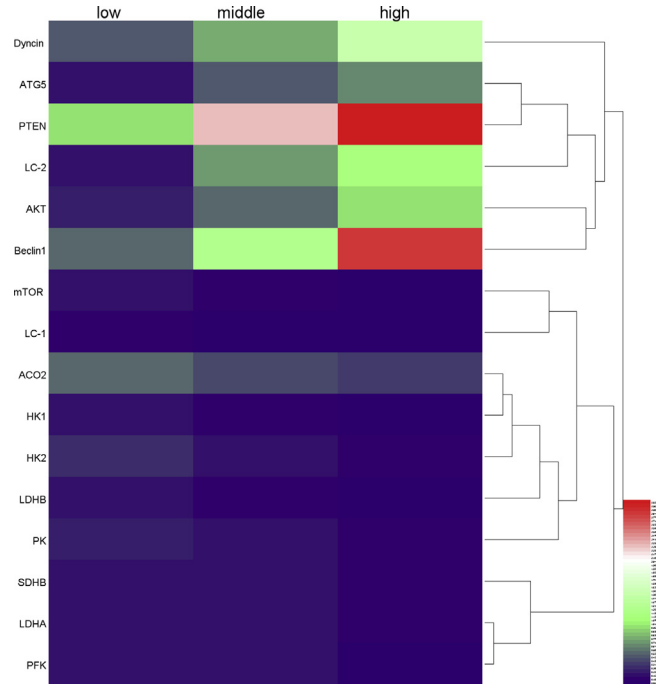

Figure 7. Heat map showing relative mRNA levels of different genes involving in multiple signaling pathways including glucose metabolism and autophagy. Different colors representing the expression levels of different autophagy and glucose metabolism genes in broilers BF. Red color displaying the highest expression level, white color displaying medium expression level, and blue color displaying relative lowest expression level of autophagy and glucose metabolism genes. The experimental groups including low, middle, and high NH_3-treated groups.

and glucose deprivation via inhibiting autophagy by suppressing mTOR complex 1 (Roberts et al., 2014). One study suggested that changes in glucose metabolism led to autophagy in chicken ovarian tissues (Wang et al., 2018). NH_3 exposure and *M. gallisepticum* infection reduced the levels of glucose metabolism–related factors in chicken neutrophils lungs (Wang et al., 2019; Ishfaq et al., 2020). While our findings (Figure 4) displayed the reduced mRNA and protein levels of glucose metabolism factors (ACO-2, HK-1, HK-2, LDHA, LDHB, PK, PFK, and SDHB) in NH_3-treated groups.

Autophagy, a phenomenon, takes place through proteins and damaged organelles (Codogno and Meijer, 2005). The suppression of mTOR signaling activated autophagy (Shang and Wang, 2011). mTOR, LC3-I, LC3-II, Dynein, Baclin-1, and ATG-5 play important roles in autophagy regulation (Yue et al., 2003; Kimmey et al., 2015; Yin et al., 2017). A previous study demonstrated that excessive cadmium and baicalin alleviated the mRNA and protein levels of AGT-5, Baclin-1, LC3-I, LC3-II, and Dynein, and decrease in mTOR level led to autophagy in rat liver and chicken BF (Zou et al., 2015; Ishfaq et al., 2021). According to our previous study, NH_3 induced autophagy in chicken hearts and thymus by increasing mRNA levels of AGT-5, Baclin-1, LC3-I, LC3-II, Dynein, and AKT and by decreasing mRNA and protein levels of mTOR (Xing et al., 2019a; Shah et al., 2020c). NH_3 exposure increased (Figure 6) the expression levels of autophagic factors except mTOR, indicating that NH_3 caused autophagy in chicken BF.

miRNAs Participate in the regulation of posttranscriptional gene expression and have been reported as autophagy regulator in many studies (Maejima et al., 2013; Gargalionis et al., 2014; Hayden et al., 2018; Ke et al., 2018). Similar to miR-181b involved in the regulation of autophagy by targeting PTEN (Li et al., 2018a), miR-93-5p was also involved in the regulation of autophagy of retinal ganglion cells by targeting PTEN (Li et al., 2018b). Our previous study demonstrated the involvement of miR-202-5p by targeting PTEN-induced autophagy in chickens' hearts after NH_3 exposure (Xing et al., 2019a). In the present study, formation of autophagosomes/autophagic lysosomes in cytoplasm (Figure 1) reduced $CD8^+$ B-lymphocyte (Figure 2) and increased expression of PTEN (Figure 5) displaying their involvement in the mediation of autophagy by activating AKT/mTOR signaling pathway in chicken BF. In addition, miR-99a-3p expression (Figure 5) was decreased, which also determined that miR-99a-3p was negatively correlated with PTEN (Figure 5).

Based on the aforementioned discussion, we predicted that PTEN is the target gene of miR-99a-3p. Our results indicated that miR-99a-3p took part in NH_3 exposure–induced autophagy in chicken BF by targeting PTEN.

CONCLUSION

In conclusion, the present study displayed that high concentration of NH_3 exposure can induce autophagy with the formation of autophagosomes/lysosomes in cytoplasm, reduced $CD8^+$ B-lymphocyte level, attenuated ATPase activities, and altered glucose metabolism, autophagy-related factors, miR-99a-3p, and its target gene PTEN in chicken BF tissues. In addition, miR-99a-3p and energy metabolism participated in NH_3-caused autophagy in chicken BF. Taken together, our results provided a new insight of risk assessment of NH_3 toxic mechanism.

ACKNOWLEDGEMENT

The present study was supported by National Natural Science Foundation of China (no. 31972612), National Key Research and Development Program of China (no. 2016YFD0500501), Smart Agricultural Engineering Research Center of Jilin Province Foundation of China, and Digital Agriculture key discipline of Jilin Province Foundation of China.

DISCLOSURES

The authors declared that there are no conflicts of interest.

REFERENCES

An, Y., H. Xing, Y. Zhang, P. Jia, X. Gu, and X. Teng. 2019. The evaluation of potential immunotoxicity induced by environmental pollutant ammonia in broilers. Poult. Sci. 98:3165–3175.

Backes, A. M., A. Aulinger, J. Bieser, V. Matthias, and M. Quante. 2016. Ammonia emissions in Europe, part II: how ammonia emission abatement strategies affect secondary aerosols. Atmos. Environ. 126:153–161.

Behera, S. N., M. Sharma, V. P. Aneja, and R. Balasubramanian. 2013. Ammonia in the atmosphere: a review on emission sources, atmospheric chemistry and deposition on terrestrial bodies. Environ. Sci. Pollut. Res. Int. 20:8092–8131.

Chen, D., G. Hu, S. Zhang, H. Zhang, and X. Teng. 2020b. Ammonia-triggered apoptosis via immune function and metabolic process in the thymuses of chickens by proteomics analysis. Ecotoxicol. Environ. Saf. 198:110619.

Chen, C., J. Li, W. Zhang, S. W. A. Shah, and M. Ishfaq. 2020a. Mycoplasma gallisepticum triggers immune damage in the chicken thymus by activating the TLR-2/MyD88/NF-κB signaling pathway and NLRP3 inflammasome. Vet. Res. 51:52.

Chen, D., Z. Miao, M. Peng, H. Xing, H. Zhang, and X. Teng. 2019. The co-expression of circRNA and mRNA in the thymuses of chickens exposed to ammonia. Ecotoxicol. Environ. Saf. 176:146–152.

Chen, D., F. Ning, J. Zhang, Y. Tang, and X. Teng. 2020c. NF-κB pathway took part in the development of apoptosis mediated by miR-15a and oxidative stress via mitochondrial pathway in ammonia-treated chicken splenic lymphocytes. Sci. Total Environ. 729:139017.

Chen, J., S. Zhang, J. Tong, X. Teng, Z. Zhang, S. Li, and X. Teng. 2020d. Whole transcriptome-based miRNA-mRNA network analysis revealed the mechanism of inflammation-immunosuppressive damage caused by cadmium in common carp spleens. Sci. Total Environ. 717:137081.

Codogno, P., and A. J. Meijer. 2005. Autophagy and signaling: their role in cell survival and cell death. Cell Death Differ. 12:1509–1518.

Coltart, I., T. H. Tranah, and D. L. Shawcross. 2013. Inflammation and hepatic encephalopathy. Arch. Biochem. Biophys. 536:189–196.

Deretic, V., T. Saitoh, and S. Akira. 2013. Autophagy in infection, inflammation and immunity. Nat. Rev. Immunol. 13:722–737.

Eng, C. H., K. Yu, J. Lucas, E. White, and R. T. Abraham. 2010. Ammonia derived from glutaminolysis is a diffusible regulator of autophagy. Sci. Signal. 3:ra31.

Gargalionis, A. N., E. K. Basdra, and A. G. Papavassiliou. 2014. MicroRNAs in colorectal neoplasia: from pathobiology to clinical applications. Curr. Pharm. Biotechnol. 15:468–474.

Han, Q., J. Tong, Q. Sun, X. Teng, H. Zhang, and X. Teng. 2020a. The involvement of miR-6615-5p/Smad7 axis and immune imbalance in ammonia-caused inflammatory injury via NF-κB pathway in broiler kidneys. Poult. Sci. 99:5378–5388.

Han, Q., J. Zhang, Q. Sun, Y. Xu, and X. Teng. 2020b. Oxidative stress and mitochondrial dysfunction involved in ammonia-induced nephrocyte necroptosis in chickens. Ecotoxicol. Environ. Saf. 203:110974.

Hayden, R., R. Flannigan, A. Mielnik, A. Bolyakov, P. Schlegel, and D. P. Urology. 2018. Discrepancies in miRNA-Seq and RT-PCR leads to discovery of high prevalence of miR-202-5P isomers in human testis. Fertil. Steril 110:e164.

Hu, X., Q. Chi, Q. Liu, D. Wang, Y. Zhang, and S. Li. 2019. Atmospheric H_2S triggers immune damage by activating the TLR-7/MyD88/NF-κB pathway and NLRP3 inflammasome in broiler thymus. Chemosphere 237:124427.

Hu, W., W. Zhang, S. W. A. Shah, M. Ishfaq, and J. Li. 2020. Mycoplasma gallisepticum infection triggered histopathological changes, oxidative stress and apoptosis in chicken thymus and spleen. Dev. Comp. Immunol. 114:103832.

Ishfaq, M., W. Zhang, S. W. Ali Shah, Z. Wu, J. Wang, L. Ding, and J. Li. 2020. The effect of Mycoplasma gallisepticum infection on energy metabolism in chicken lungs: through oxidative stress and inflammation. Microb. Pathog. 138:103848.

Ishfaq, M., W. Zhang, W. Hu, S. Waqas Ali Shah, Y. Liu, J. Wang, Z. Wu, I. Ahmad, and J. Li. 2019. Antagonistic effects of baicalin on *Mycoplasma gallisepticum*-induced inflammation and apoptosis by restoring energy metabolism in the chicken lungs. Infect. Drug Resist. 12:3075–3089.

Ishfaq, M., W. Zhang, Y. Liu, J. Wang, Z. Wu, S. W. Shah, R. Li, Y. Miao, C. Chen, and J. Li. 2021. Baicalin attenuated *Mycoplasma gallisepticum*-induced immune impairment in chicken bursa of fabricius through modulation of autophagy and inhibited inflammation and apoptosis. J. Sci. Food Agric. 101:880–890.

Jayachandra, K., T. A. Kannan, S. H. Basha, A. Raja, and G. Ramesh. 2017. Flow cytometric analysis of T cell subset in bursa of fabricius in broiler chicken (Gallus domesticus). Int. J. Curr. Microbiol. Appl. Sci. 6:1534–1539.

Ke, S. B., H. Qiu, J. M. Chen, W. Shi, and Y. S. Chen. 2018. MicroRNA-202-5p functions as a tumor suppressor in colorectal carcinoma by directly targeting SMARCC1. Gene 676:329e335.

Kimmey, J. M., J. P. Huynh, L. A. Weiss, S. Park, A. Kambal, J. Debnath, H. W. Virgin, and C. L. Stallings. 2015. Unique role for ATG5 in neutrophil-mediated immunopathology during M. tuberculosis infection. Nature 528:565–569.

Kristensen, H. H., and C. M. Wathes. 2000. Ammonia and poultry welfare: a review. Worlds Poult. Sci. J. 56:235–245.

Kroemer, G., G. Mariño, and B. Levine. 2010. Autophagy and the integrated stress response. Mol. Cell 40:280–293.

Li, W., Y. Jiang, Y. Wang, S. Yang, X. Bi, X. Pan, A. Ma, and W. Li. 2018a. MiR-181b regulates autophagy in a model of Parkinson's disease by targeting the PTEN/Akt/mTOR signaling pathway. Neurosci. Lett. 675:83–88.

Li, R., Y. Jin, Q. Li, X. Sun, H. Zhu, and H. Cui. 2018b. MiR-93-5p targeting PTEN regulates the NMDA-induced autophagy of retinal ganglion cells via AKT/mTOR pathway in glaucoma. Biomed. Pharmacother. 100:1–7.

Li, J., Z. Qiao, W. Hu, W. Zhang, S. W. A. Shah, and M. Ishfaq. 2019. Baicalin mitigated Mycoplasma gallisepticum-induced structural damage and attenuated oxidative stress and apoptosis in chicken thymus through the Nrf2/HO-1 defence pathway. Vet. Res. 50:83.

Li, Q., J. Xie, R. Li, J. Shi, J. Sun, R. Gu, L. Ding, L. Wang, and B. Xu. 2014. Overexpression of microRNA-99a attenuates heart remodelling and improves cardiac performance after myocardial infarction. J. Cell Mol. Med. 18:919–928.

Lock, R., S. Roy, C. M. Kenific, J. S. Su, E. Salas, S. M. Ronen, and J. Debnath. 2011. Autophagy facilitates glycolysis during Ras-mediated oncogenic transformation. Mol. Biol. Cell 22:165–178.

Lucocq, J. M., and C. Hacker. 2013. Cutting a fine figure: on the use of thin sections in electron microscopy to quantify autophagy. Autophagy 9:1443–1448.

Luo, C., G. Shen, N. Liu, F. Gong, X. Wei, S. Yao, D. Liu, X. Teng, N. Ye, N. Zhang, X. Zhou, J. Li, L. Yang, X. Zhao, L. Yang, R. Xiang, and Y. Q. Wei. 2014. Ammonia drives dendritic cells into dysfunction. J. Immunol. 193:1080–1089.

Maejima, Y., S. Kyoi, P. Zhai, T. Liu, H. Li, A. Ivessa, S. Sciarretta, D. P. Del Re, D. K. Zablocki, C. P. Hsu, D. S. Lim, M. Isobe, and J. Sadoshima. 2013. Mst1 inhibits autophagy by promoting the interaction between Beclin1 and Bcl-2. Nat. Med. 19:1478–1488.

Moruno-Manchón, J. F., E. Pérez-Jiménez, and E. Knecht. 2013. Glucose induces autophagy under starvation conditions by a p38 MAPK-dependent pathway. Biochem. J. 449:497–506.

Naseem, S., and A. J. King. 2018. Ammonia production in poultry houses can affect health of humans, birds, and the environment—techniques for its reduction during poultry production. Environ. Sci. Pollut. Res. Int. 25:15269–15293.

Pant, K., A. Saraya, and S. K. Venugopal. 2017. Oxidative stress plays a key role in butyrate-mediated autophagy via Akt/mTOR pathway in hepatoma cells. Chem. Biol. Interact. 273:99–106.

Pfaffl, M. W. 2001. A new mathematical model for relative quantification in real-time RT-PCR. Nucleic Acids Res. 29:45e45.

Roberts, D. J., V. P. Tan-Sah, E. Y. Ding, J. M. Smith, and S. Miyamoto. 2014. Hexokinase-II positively regulates glucose starvation-induced autophagy through TORC1 inhibition. Mol. Cell 53:521–533.

Rule, C. S., M. Patrick, and M. Sandkvist. 2016. Measuring in vitro ATPase activity for enzymatic characterization. J. Vis. Exp. 54305.

Shah, S. W. A., J. Chen, Q. Han, Y. Xu, M. Ishfaq, and X. Teng. 2020a. Ammonia inhalation impaired immune function and mitochondrial integrity in the broilers bursa of fabricius:

implication of oxidative stress and apoptosis. Ecotoxicol. Environ. Saf. 190:110078.

Shah, S. W. A., D. Chen, J. Zhang, Y. Liu, M. Ishfaq, Y. Tang, and X. Teng. 2020c. The effect of ammonia exposure on energy metabolism and mitochondrial dynamic proteins in chicken thymus: through oxidative stress, apoptosis, and autophagy. Ecotoxicol. Environ. Saf. 206:111413.

Shah, S. W. A., M. Ishfaq, M. Nasrullah, A. Qayum, M. U. Akhtar, H. Jo, M. Hussain, and X. Teng. 2020b. Ammonia inhalation-induced inflammation and structural impairment in the bursa of fabricius and thymus of broilers through NF-κB signaling pathway. Environ. Sci. Pollut. Res. Int. 27:11596–11607.

Shang, L., and X. Wang. 2011. AMPK and mTOR coordinate the regulation of Ulk1 and mammalian autophagy initiation. Autophagy 7:924–926.

Shi, Q., X. Jin, R. Fan, M. Xing, J. Guo, Z. Zhang, J. Zhang, and S. Xu. 2018. Cadmium-mediated miR-30a-GRP78 leads to JNK-dependent autophagy in chicken kidney. Chemosphere 215:710–715.

Singh, S. V., A. N. Dakhole, A. Deogharkar, S. Kazi, R. Kshirsagar, A. Goel, A. Moiyadi, R. Jalali, E. Sridhar, T. Gupta, P. Shetty, N. Gadewal, and N. V. Shirsat. 2017. Restoration of miR-30a expression inhibits growth, tumorigenicity of medulloblastoma cells accompanied by autophagy inhibition. Biochem. Biophys. Res. Commun. 491:946–952.

Sun, J., W. Shengchen, C. Yirong, W. Shuting, and L. Shu. 2020. Cadmium exposure induces apoptosis, inflammation and immunosuppression through CYPs activation and antioxidant dysfunction in common carp neutrophils. Fish Shellfish Immunol. 99:284–290.

Sutton, M., U. Dragosits, Y. Tang, and D. Fowler. 2000. Ammonia emissions from non-agricultural sources in the UK. Atmos. Environ. 34:855–869.

Tranah, T. H., G. K. Vijay, J. M. Ryan, and D. L. Shawcross. 2013. Systemic inflammation and ammonia in hepatic encephalopathy. Metab. Brain Dis. 28:1–5.

Tsai, T. F., J. F. Lin, K. Y. Chou, Y. C. Lin, H. E. Chen, and T. I. S. Hwang. 2018. miR-99a-5p acts as tumor suppressor via targeting to mTOR and enhances RAD001-induced apoptosis in human urinary bladder urothelial carcinoma cells. Oncotargets Ther. 11:239–252.

Tualeka, A. R., and J. Jalaludin. 2018. Observation of adverse effect on level ammonia through expression of CD8 lymphocyte in mice. Mal. J. Med. Health Sci. 14:71–77.

Wang, S., X. Li, W. Wang, H. Zhang, and S. Xu. 2019. Application of transcriptome analysis: oxidative stress, inflammation and microtubule activity disorder caused by ammonia exposure may be the primary factors of intestinal microvilli deficiency in chicken. Sci. Total Environ. 696:34035.

Wang, L., L. Wang, X. Shi, and S. Xu. 2020. Chlorpyrifos induces the apoptosis and necroptosis of L8824 cells through the ROS/PTEN/PI3K/AKT axis. J. Hazard. Mater. 398:122905.

Wang, S., Z. Xu, H. Yin, Y. Min, and S. Li. 2018. Alleviation mechanisms of selenium on cadmium-spiked in chicken ovarian tissue: perspectives from autophagy and energy metabolism. Biol. Trace Elem. Res. 186:521–528.

Wang, D., Y. Zhang, Q. Chi, X. Hu, S. Li, and S. Li. 2019. Ammonia exposure induced abnormal expression of cytokines and heat shock proteins via glucose metabolism disorders in chicken neutrophils. Environ. Sci. Pollut. Res. Int. 26:10529–10536.

Xing, H., J. Chen, M. Peng, Z. Wang, F. Liu, S. Li, and X. Teng. 2019b. Identification of signal pathways for immunotoxicity in the spleen of common carp exposed to chlorpyrifos. Ecotoxicol. Environ. Saf. 182:109464.

Xing, H., M. Peng, Z. Li, J. Chen, H. Zhang, and X. Teng. 2019a. Ammonia inhalation-mediated mir-202-5p leads to cardiac autophagy through PTEN/AKT/mTOR pathway. Chemosphere 235:858–866.

Xu, X., K. Araki, S. Li, J. H. Han, L. Ye, W. G. Tan, B. T. Konieczny, M. W. Bruinsma, J. Martinez, E. L. Pearce, D. R. Green, D. P. Jones, H. W. Virgin, and R. Ahmed. 2014. Autophagy is essential for effector CD8+ T cell survival and memory formation. Nat. Immunol. 15:1152–1161.

Xu, Y., Z. Li, S. Zhang, H. Zhang, and X. Teng. 2020. miR-187-5p/apaf-1 axis was involved in oxidative stress-mediated apoptosis caused by ammonia via mitochondrial pathway in chicken livers. Toxicol. Appl. Pharmacol. 388:114869.

Yan, L., Z. Chen, L. Wu, Y. Su, X. Wang, and N. Tang. 2018. Inhibitory effect of PXR on ammonia-induced hepatocyte autophagy via P53. Toxicol. Lett. 295:153–161.

Yi, B., L. Chen, R. Sa, R. Zhong, H. Xing, and H. Zhang. 2016. High concentrations of atmospheric ammonia induce alterations of gene expression in the breast muscle of broilers (Gallus gallus) based on RNA-Seq. BMC Genomics 17:598–609.

Yin, H., L. Zhao, S. Li, L. Xu, Y. Wang, and H. Chen. 2017. Impaired cellular energy metabolism contributes to duck-enteritis-virus-induced autophagy via the AMPK–TSC2–MTOR signaling pathway. Front. Cell Infect. Microbiol. 7.

Yue, Z., S. Jin, C. Yang, A. J. Levine, and N. Heintz. 2003. Beclin 1, an autophagy gene essential for early embryonic development, is a haploinsufficient tumor suppressor. Proc. Natl. Acad. Sci. U. S. A. 100:15077–15082.

Zhang, J., C. Li, X. Tang, Q. Lu, R. Sa, and H. Zhang. 2015. Proteome changes in the small intestinal mucosa of broilers (Gallus gallus) induced by high concentrations of atmospheric ammonia. Proteome Sci. 13:9.

Zhang, Y., Q. Liu, H. Yin, and S. Li. 2020. Cadmium exposure induces pyroptosis of lymphocytes in carp pronephros and spleens by activating NLRP3. Ecotoxicol. Environ. Saf. 202:110903.

Zhang, W., Y. Liu, Q. Zhang, S. Waqas Ali Shah, Z. Wu, J. Wang, M. Ishfaq, and J. Li. 2020. *Mycoplasma gallisepticum* infection impaired the structural integrity and immune function of bursa of fabricius in chicken: implication of oxidative stress and apoptosis. Front. Vet. Sci. 7:225.

Zou, H., L. Zhuo, T. Han, D. Hu, X. Yang, Y. Wang, Y. Yuan, J. Gu, J. Bian, X. Liu, and Z. Liu. 2015. Autophagy and gap junctional intercellular communication inhibition are involved in cadmium-induced apoptosis in rat liver cells. Biochem. Biophys. Res. Commun. 459:713–719.